Mass fractionation processes of transition metal isotopes

X.K. Zhu [a,*], Y. Guo [a], R.J.P. Williams [b], R.K. O'Nions [a], A. Matthews [a,c],
N.S. Belshaw [a], G.W. Canters [d], E.C. de Waal [d], U. Weser [e], B.K. Burgess [f,1],
B. Salvato [g]

[a] *Department of Earth Sciences, University of Oxford, Parks Road, Oxford OX1 3PR, UK*
[b] *Department of Chemistry, University of Oxford, South Parks Road, Oxford OX1 3QR, UK*
[c] *Institute of Earth Sciences, Hebrew University of Jerusalem, 91904 Jerusalem, Israel*
[d] *Leiden Institute of Chemistry, Leiden University, Einsteinweg 55, 2333 CC Leiden, The Netherlands*
[e] *Anorganische Biochemie, Physiologisch-Chemische Institut, Eberhard-Karls-Universität Tübingen, Hoppe-Seyler-Str. 4,
D-72076 Tübingen, Germany*
[f] *Department of Molecular Biology and Biochemistry, University of California, Irvine, CA 92717, USA*
[g] *CNR Centre of Metalloproteins, Padua University, I-35121 Padua, Italy*

Abstract

Recent advances in mass spectrometry make it possible to utilise isotope variations of transition metals to address some important issues in solar system and biological sciences. Realisation of the potential offered by these new isotope systems however requires an adequate understanding of the factors controlling their isotope fractionation. Here we show the results of a broadly based study on copper and iron isotope fractionation during various inorganic and biological processes. These results demonstrate that: (1) naturally occurring inorganic processes can fractionate Fe isotope to a detectable level even at temperature $\sim 1000°C$, which challenges the previous view that Fe isotope variations in natural system are unique biosignatures; (2) multiple-step equilibrium processes at low temperatures may cause large mass fractionation of transition metal isotopes even when the fractionation per single step is small; (3) oxidation–reduction is an importation controlling factor of isotope fractionation of transition metal elements with multiple valences, which opens a wide range of applications of these new isotope systems, ranging from metal-silicate fractionation in the solar system to uptake pathways of these elements in biological systems; (4) organisms incorporate lighter isotopes of transition metals preferentially, and transition metal isotope fractionation occurs stepwise along their pathways within biological systems during their uptake. © 2002 Elsevier Science B.V. All rights reserved.

Keywords: stable isotopes; fractionation; metals; proteins; iron; copper

1. Introduction

Natural variations in stable isotope abundances of light elements such as O, H, C, and S, have over the years provided profound insights into

---

* Corresponding author.
E-mail address: xiangz@earth.ox.ac.uk (X.K. Zhu).

[1] Deceased.

processes operating during the formation of the solar system, the evolution of the Earth, and interactions between geosphere and biosphere. Due to the revolutionary developments in mass spectrometry over the last few years [1–10], stable isotope abundances of heavier elements are now accessible, and investigation of isotope variations of transition metals such as Fe, Cu, Zn and Mo, has become a new and fast developing research area. Pioneering studies have demonstrated that potential exists for applications of transition metal isotope systems from cosmochemistry, geochemistry, through organic and inorganic chemistry, to biochemistry and the environment [3–6,9–13]. However, realisation of this potential is hampered by our inadequate knowledge about the processes which control the mass fractionation of these isotope systems, although initial results suggest that both biological and abiotic processes may be important for Fe and Cu isotopes [4,10–19].

Here we report investigations on Cu and Fe isotope fractionation during various processes. This study expands our knowledge about transition metal isotope fractionation processes significantly, and provides a basis for a wide range applications of these new isotope systems.

2. Inorganic mass fractionation at high temperatures

Whether or not naturally occurring inorganic processes fractionate transition metal isotopes is an issue of current debate [2–6,8,10–19]. Although it has been claimed that natural Fe isotope variation is a unique biological signature [3,11], there is strong evidence to suggest that Fe and Cu isotopes may be fractionated abiotically in low temperature environments [2,4,8,13,17]. However, the critical question remains as to whether Fe isotopes can be fractionated by pure inorganic processes taking place in nature, especially by equilibrium processes. To investigate this issue, Fe isotope compositions of natural materials have been measured, where biological involvement was most unlikely, and the mineral phases were most likely to be in equilibrium.

2.1. Samples and methods

The samples chosen for this study are mantle lherzolite xenoliths and pallasite meteorites. Lherzolite xenoliths are samples of the upper mantle carried to the Earth's surface through volcanism. Three mantle xenoliths, namely TKN31F, JL1 and BD3855, were selected. They are spinel lherzolites and consist predominantly of olivine, orthopyroxene and clinopyroxene. TKN31F is from Boss Mountain, and JL1 from Jacques Lake, central British Columbia, Canada [20–22]. Minerals in these two samples are equilibrated at c. 1000°C [20–22]. BD3855 is from Pello Hill, Tanzania, where the xenoliths have been subjected to mantle metasomatism [23]. Pallasite is a group of meteorites which consists predominantly of Fe–Ni alloy and olivine. These minerals have crystallised from melts in the interiors of asteroid-sized parent bodies. Two samples were chosen for this study. They are Imilac, which belongs to the main group pallasite, and Eagle Station, which belongs to the non-main group pallasite.

Samples were gently crushed and minerals of olivine, orthopyroxene, clinopyroxene, and the metal phase were handpicked. Amphibole was separated from a metasomatic vein in BD3855. The mineral separates were cleaned in purified water in an ultrasonic bath. Silicate minerals were digested using concentrated HF and HNO_3 mixture, and the Fe–Ni alloys were dissolved in 6 M HCl. All samples were subsequently purified chromatographically as described in Appendix A. The purified samples were measured for Fe isotopes on a Nu Instruments plasma source mass spectrometer in the Earth Science Department, Oxford. Details of the mass spectrometry are presented in Appendix A.

2.2. Results and implications

Results are expressed in terms of $\varepsilon^{56}Fe$ and $\varepsilon^{57}Fe$, which are deviations in parts per 10^4 from the Fe isotope reference material IRMM-14. For the mantle xenoliths, Fe isotopes vary from −1.8 to 5.5 $\varepsilon^{57}Fe$ units (Table 1). The results show no detectable isotope fractionation between clinopyroxene and orthopyroxene in each sample.
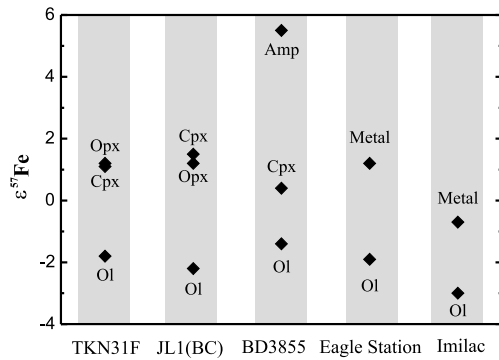
Fig. 1. A plot showing phase-related variation of Fe isotopes in mantle xenoliths and pallasites. All results for ε^{57}Fe are relative to IRMM-14 standard. The size of data symbols represents approximately the external precision at 1σ level. Ol-olivine; Opx-orthopyroxene; Cpx-clinopyroxene; Amp-amphibole.

Relative to pyroxenes, however, the Fe isotope composition in olivine is systematically lighter (Fig. 1), with fractionation between olivine and clinopyroxene varying from 1.8 to 3.7 ε^{57}Fe

units. Amphibole in BD3855 shows the heaviest Fe isotope composition in all these mineral phases.

Whereas the amphibole in BD3855 is a product of metasomatism and may not be in equilibrium, minerals in the other two samples were equilibrated [20–22]. In fact, the observed pattern of Fe isotopes in olivine and pyroxenes is similar to the equilibrium distribution of oxygen isotopes in mantle peridotite, where the oxygen isotope composition of olivine is systematically lighter than that of clinopyroxene and orthopyroxene [24]. Moreover, Mg isotopes in these samples have also been measured in this laboratory, and show a similar variation between these mineral phases (A. Galy, 2001, personal communication). Thus it is concluded that the heavy isotope enrichment in pyroxenes relative to olivine results from equilibrium partitioning of Fe isotopes between these minerals, whereas the large difference in Fe isotope composition between amphibole and other mineral phases possibly point to the impor-

Table 1
Fe isotope results of mantle xenoliths and pallasites

Sample	Mineral phase	ε^{57}Fe[a]	ε^{56}Fe[a]
Mantle xenoliths			
TKN 31F	Olivine	−1.8	−1.2
TKN 31F	Orthopyroxene	1.2	0.8
TKN 31F	Clinopyroxence	1.1	0.8
JL1 (BC)	Olivine	−2.2	−1.8
JL1 (BC)	Orthopyroxene	1.2	0.8
JL1 (BC)	Clinopyroxence	1.5	1.1
BD3855	Olivine	−1.4	−1.0
BD3855	Clinopyroxence	0.4	0.2
BD3855	Amphibole	5.8	3.6
BD3855	Amphibole[b]	5.2	3.2
Pallasites			
Eagle Station	Metal fraction	1.2	0.7
Eagle Station	Olivine	−1.9	−1.2
Imilac	Metal	−0.7	−0.5
Imilac	Olivine	−3.0	−1.9

All results are relative to IRMM-14 Fe isotope standard.
[a] Measured ^{57}Fe/^{54}Fe and ^{56}Fe/^{54}Fe ratios are expressed as ε^{57}Fe and ε^{56}Fe, which are deviations in parts per 10^4 from the Fe isotope reference material IRMM-14 as follows:

$$\varepsilon^X\text{Fe} = \left(\frac{R_{\text{sample}}}{R_{\text{standard}}}-1\right)\times 10000$$

, where $R = {}^X$Fe/^{54}Fe. Values of ε^{56}Fe and ε^{57}Fe for each sample are the averages of two or three separate analyses. External precision at 2σ level is 0.4ε and 0.6ε for ε^{56}Fe and ε^{57}Fe, respectively (see Appendix A).
[b] Duplicate analysis including duplication of ion exchange chromatographic separation.

tance of kinetic processes in isotope mass frac-
tionation even at high temperatures.

For the pallasite samples, an overall variation
of c. 4 ε^{57}Fe units has been observed, with
$-3 \leq \varepsilon^{57}$Fe ≤ 1.2 (Table 1). As for the mantle
xenoliths, this variation is also phase-related
(Fig. 1). Relative to olivine, the metal phase
shows heavy isotope enrichment in both samples.
This variation trend is consistent with theoretical
calculations of Fe isotope fractionation based on
Mössbauer spectrometry [19].

It is well known that equilibrium mass fraction-
ation of stable isotopes is expected to become
smaller with the increase of temperature and
decrease of the relative mass difference between
the isotopes [25,26]. Given the very high tem-
peratures at which these minerals are expected
to have been equilibrated, the existence of detect-
able mass fractionation in these mineral phases
is remarkable. These results demonstrate that nat-
urally occurring inorganic processes can fraction-
ate transition metal isotopes to significant levels
even at temperatures of c. 1000°C, and they point
out further that much larger mass fractionations
may be expected from equilibrium inorganic pro-
cesses at lower temperatures. These results, to-
gether with some previous studies [6,13,14], dem-
onstrate that Fe isotope composition cannot be
used uncritically as a unique biological signature
in search of ancient or extraterrestrial life as pre-
viously suggested. Moreover, metal-silicate frac-
tionation is a fundamental process during solar
nebular and planetary evolution. The systematic
difference in Fe isotope composition between ol-
ivine and metal phases in the analysed pallasites
shows that metal-silicate separation does cause
Fe isotope fractionation. Thus the Fe isotope
composition may in turn throw light on this im-
portant process during the early solar system evo-
lution.

3. Equilibrium fractionation in aqueous solutions

One straightforward approach to the study of
isotope fractionation between equilibrated species
in aqueous solutions is to use ion exchange chro-
matography. During a chromatographic process,

ions in solution partition themselves between the
stationary resin and the mobile aqueous phase.
According to plate theory [27–29], an ion ex-
change chromatographic column can be consid-
ered as a number of theoretical plates, where
each plate is the equivalent of a single chemical
step at equilibrium.

The approach of using chromatography to
study isotope fractionation per single separation
step (plate) at equilibrium was initially put on a
theoretical basis by Glueckauf [29], and was sub-
sequently employed to study chromatographic
fractionation of Ca and Fe isotopes [16,30]. In
this study, we used a strongly basic anion ex-
change resin (AG-MP1) to investigate the equilib-
rium fractionation of Cu isotopes in 6 M HCl
solutions. In such solution, Cu^{2+} chloro-com-
plexes are present dominantly as $CuCl_4^{2-}$ [31–
33]. According to the plate theory [27–29], equi-
librium mass fractionation of Cu isotopes between
their resin bound chloro-complex and the free
chloro-complex of $CuCl_4^{2-}$ in 6 M HCl solutions
equals that produced per single theoretical plate
during chromatographic processes.

The chromatographic experiments were carried
out at room temperature (c. 20°C). The procedure
for Cu isotope mass spectrometry has been de-
scribed elsewhere [4], and the measured results
are expressed in terms of ε^{65}Cu units which are
deviations in 10^4 relative to the experimental
stock solution. As shown in Fig. 2A, large mass
fractionation of Cu isotopes is induced by an ion
exchange process, consistent with previous obser-
vations [2]. Following the classic treatment
[16,29,30], the enrichment factor of the heavier
Cu isotope per single plate is $\beta = 7.5 \times 10^{-4}$ (Fig.
2B). This implies that the heavier Cu isotope is
enriched in the resin bound $CuCl_4^{2-}$ species by 7.5
ε^{65}Cu units per single step under the experimental
conditions.

These results demonstrate that detectable frac-
tionations of Cu isotopes can occur in low tem-
perature aqueous environments even between
equilibrated species where differences in bonding
strengths are very small. Furthermore, the above
results, together with a previous study [16], show
that large fractionation can be achieved for both
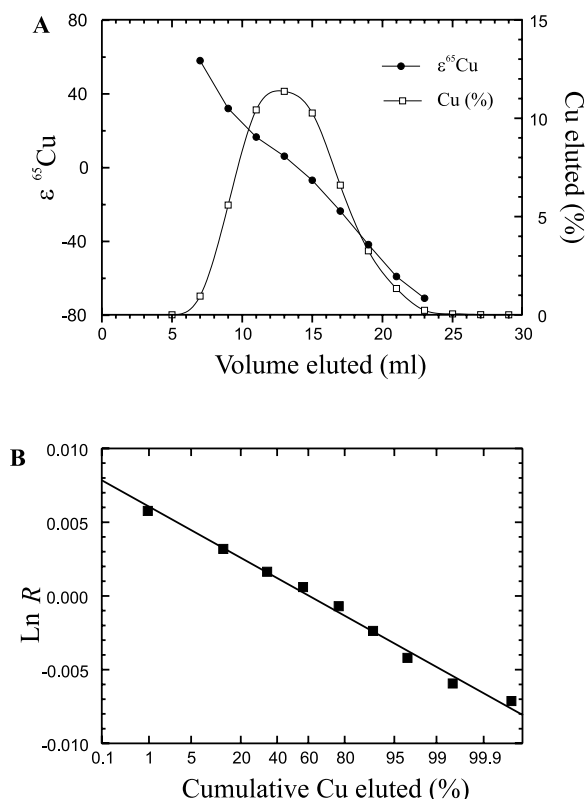Cu and Fe isotopes by multiple-step processes

Fig. 2. Equilibrium mass fractionation of Cu isotopes between aqueous species during ion exchange chromatography. (A) ε^{65}Cu values for Cu eluted from an ion exchange column using anion resin AG-MP1. The overall isotope fractionation that occurred during the chromatographic process is considered to result from multiple step equilibrium fractionation between the resin bound $CuCl_4^{2-}$ and the free $CuCl_4^{2-}$ species. From an ideal Gaussian elution curve, the number of steps (i.e., the number of theoretical plates), N, is obtained from the relation $N = 5.54 \times (V_R/W_{1/2})^2$ where V_R is the volume to the curve peak and $W_{1/2}$ is the width of the curve at half-height [27]. If the tailing effect is neglected, then $N = 12$. (B) Cu isotope compositions in elution fractions, R, vs. cumulative percentage of Cu eluted on a normal deviate (probability) scale. $R = (^{65}Cu/^{63}Cu)_{fraction}/(^{65}Cu/^{63}Cu)_{total}$. The slope b on such a plot reflects the extent of isotope separation during elution, and $b \approx -\beta\sqrt{N}$, where N is the number of theoretical plates in the column, and β is the enrichment factor per single plate [29]. The line represents a best visual fit to the data.

even when the equilibrium fractionation per single step is small.

4. Mass fractionation during redox-related processes

Oxidation–reduction is a fundamental aspect of the geochemistry and biochemistry of transition metals such as Cu, Fe, Ni, Cr and Mo. The isotope fractionation between olivine and metal phases in pallasite samples described above is in essence a redox-related process. More recently, it has been shown that Fe isotope fractionation may be induced by abiotic redox process in aqueous environments [13]. Here Cu is taken as an example to investigate transition metal isotope fractionation during redox-related processes in low temperature environments.

4.1. Experimental procedure

Experiments on Cu isotope fractionation during redox-related processes were performed at room temperature (c. 20°C), utilising the following chemical reactions:
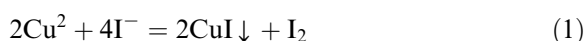
$$2Cu^2 + 4I^- = 2CuI\downarrow + I_2 \qquad (1)$$

Table 2
Results of Cu-redox experiments at room temperature (c. 20°C)

Experiment no.	Cu(NO₃)₂/KI[a] (ml/ml)	Time[b] (h)	ε^{65}Cu(II)	ε^{65}Cu(I)[c]	Δ^{65}Cu[d]	$\alpha_{Cu(II)-Cu(I)}$ [e]
Cu-redox-1	2.5/0.5	1.25	1.8	−38.7	40.5	1.00406
Cu-redox-2	2.5/0.5	1.75	1.8	−38.7	40.5	1.00406
Cu-redox-3	2.5/0.5	18	1.7	−37.8	39.5	1.00397
Cu-redox-4	2.5/0.5	18	1.4	−37.9	39.3	1.00394
Cu-redox-5	2.5/1.0	18	6.1	−35.0	41.1	1.00412
Cu-redox-6	2.5/0.3	18	0.6	−39.0	39.6	1.00397
Cu-redox-7	2.5/2.0	20	13.4	−27.4	40.8	1.00409
Cu-redox-8	2.5/1.0	20	5.6	−34.7	40.3	1.00405
Cu-redox-9	2.5/2.0	20	13.3	−27.6	40.9	1.00411
Cu-redox-10	2.5/1.5	20	8.4	−31.1	39.5	1.00397

The ε^{65}Cu results are relative to Cu stock solution.
[a] Initial solutions are 0.05 M Cu(NO₃)₂ in 0.1 M HNO₃ and 0.096 M KI in H₂O.
[b] Time allowed to stand before centrifuging.
[c] Repeated measurements of Romil Cu solution versus NIST-976 Cu isotope reference material over a period of a few months define an external precision of 0.5ε at 2σ level.
[d] Δ^{65}Cu $= \varepsilon^{65}$Cu(II)$- \varepsilon^{65}$Cu(I).
[e] Isotope fractionation factor between Cu(II) and Cu(I). The experiment results define a mean $\alpha_{Cu(II)-Cu(I)} = 1.00403 \pm 0.00004$ in diluted HNO₃ medium at c. 20°C.

The initial solutions used for the experiments were 0.05 M Cu(NO₃)₂ in 0.1 M HNO₃ and 0.096M KI in H₂O. These two solutions were mixed in various proportions, and different amounts of CuI precipitate relative to total Cu were produced. After standing for periods varying from 75 min to 20 h, the CuI precipitates were separated from the residual Cu solutions by centrifuging. The precipitates were then thoroughly washed using purified H₂O and the wash solutions were collected and combined with their corresponding Cu soluble fractions. The soluble Cu fractions were then purified using procedures described in Appendix A. The CuI precipitates were dissolved in 6M HCl, and dried down three times to convert the Cu to Cl⁻ form. The ^{65}Cu/^{63}Cu ratio was measured using a standard-sample bracketing method [4]. Results are expressed as ε^{65}Cu values relative to the Cu isotope composition of the initial Cu solution (Table 2). In that way, any isotope deviation measured must result from the chemical reaction expressed in Eq. 1.

4.2. Experimental results

The experimental results display some important features. Firstly, they demonstrate that there is significant mass fractionation between the CuI and remaining solution, and the CuI precipitates show light isotope enrichment relative to the initial isotope composition. Secondly, the isotope compositions of both CuI and remaining soluble species deviate from their initial solution as a function of Cu(NO₃)₂/KI ratio (Table 2 and Fig. 3A), paralleling the amount of Cu²⁺ remaining after reaction. Thirdly, despite the fact that the Cu(NO₃)₂/KI molar ratio varies from 0.65 to 4.34, and the time allowed for the solution to stand before centrifuging differs from 75 min to 20 h, the isotope fractionation between CuI and the remaining soluble fractions remains constant at c. 40 ε^{65}Cu units (Table 2 and Fig. 3A).

4.3. Significance of the results

The chemical reaction expressed in Eq. 1 may be considered a two-step process: reduction of Cu²⁺ to Cu⁺ and subsequent formation of insoluble CuI. In principle, both processes may induce Cu isotope fractionation. However, given the solubility product of CuI $K_{CuI} = 1.8 \times 10^{-9}$ [34], [Cu⁺] in all the remaining soluble fractions is expected to be less than 10^{-6} M for the given experimental conditions (Table 2), which is more
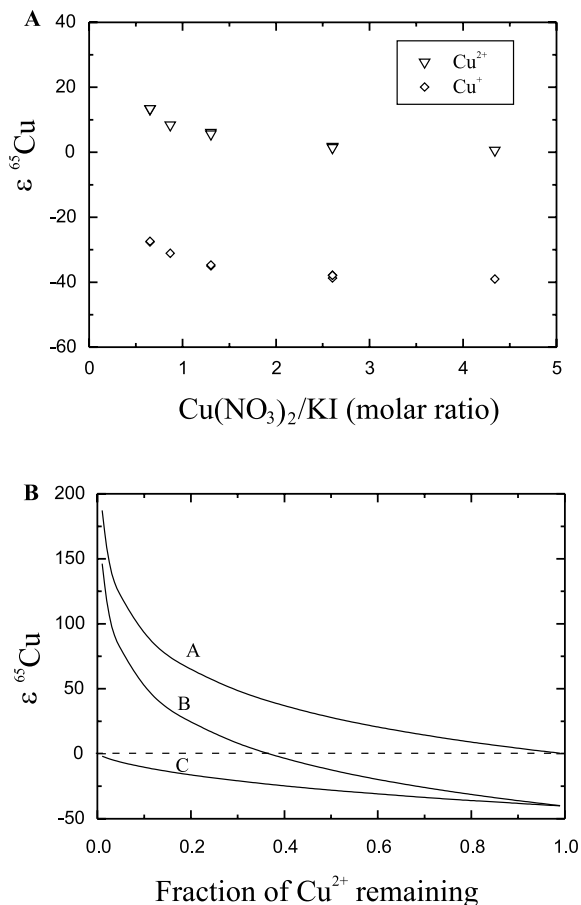
Fig. 3. (A) Experimental results of Cu isotope fractionation between Cu^+ and Cu^{2+} aqueous species at 20°C. All $\varepsilon^{65}Cu$ values are expressed relative to the original Cu solution used for the experiments. Note that the mass fractionation between Cu^{2+} solution and CuI precipitates remains constant at c. 40 ε units in $^{65}Cu/^{63}Cu$ ratio over a large range of experimental conditions. (B) Modelling results of Raleigh fractionation between Cu^{2+} and Cu^+ based on a fractionation factor between the two species $\alpha = 1.00403$ as defined by the experimental results presented in panel A. Curve A is for $\varepsilon^{65}Cu$ variation in the Cu^{2+} species remaining in solution. Curve B shows the variation of $\varepsilon^{65}Cu$ in the CuI phase precipitated in equilibrium with Cu^{2+} aqueous species from the solution. Curve C shows the change of $\varepsilon^{65}Cu$ in the accumulative CuI precipitate as a function of its accumulation. The dashed line represents the isotope composition of the initial solution. These results show three important points. Firstly, the heavy isotope enrichment in the remaining Cu^{2+} solution relative to the initial solution can be much larger than the equilibrium fractionation between Cu^{2+} and Cu^+ species. Secondly, relative to the initial solution, both Cu^{2+} and Cu^+ species can show heavy isotope enrichment. Thirdly, the overall fractionation between Cu^{2+} and Cu^+ species can be much larger than the equilibrium fractionation between the two species.
←

than four orders of magnitude lower than $[Cu^{2+}]$ in the corresponding remaining solutions. Thus the measured Cu isotope composition of the remaining solution is essentially the isotope composition of the pure Cu^{2+} species in the solution, and mass fractionation between the CuI precipitate and the remaining Cu solution is essentially induced by reduction of Cu^{2+} to Cu^+. Therefore, the above experimental results demonstrate that the oxidation–reduction process is a very important control of isotope fractionation of transition metals with multiple valences.

The fact that isotope fractionation between the Cu^{2+} and Cu^+ species remains constant despite great variations in experimental conditions strongly suggests that isotopic equilibrium was achieved between those two species in each experiment. Thus an isotope fractionation factor between the two Cu species at c. 20°C for the given experimental conditions, $\alpha_{Cu(II)-Cu(I)} = 1.00403 \pm 0.00004$, can be defined by the experiment results.

Using the fractionation factor obtained above, the significance of the results in understanding mass fractionation of transition metal isotopes during redox-related processes in natural systems may be discussed further on the basis of the Rayleigh fractionation model (Fig. 3B). According to this model, it is assumed that CuI is in isotopic equilibrium with Cu^{2+} during its formation but no further isotopic exchange occurs between the two species thereafter. Curve A represents the isotope compositional evolution of Cu^{2+} species in the remaining solution. It shows that the heavy isotope in the remaining solution is enriched progressively as its amount decreases, and the enrichment can be much larger than the equilibrium fractionation between the two species. For example, at the point where 1% Cu^{2+} remains, the heavy isotope is enriched by c. 190 $\varepsilon^{65}Cu$ units relative to the initial isotope composition. Curve B shows the variation of isotope composition of the CuI phase precipitated from the solution in equilibrium with the Cu^{2+} aqueous species. At

any given point, the isotope composition of CuI precipitate is lighter than the Cu^{2+} aqueous species by c. 40 $\varepsilon^{65}Cu$ units. Furthermore, these modelling results show that under Rayleigh fractionation it is possible for the heavy isotope to become enriched in both the CuI precipitate and the remaining Cu^{2+} aqueous species relative to the initial copper isotope composition. Curve C illustrates the isotope change of the CuI precipitate as a function of its accumulation. Under this circumstance, fractionation between the Cu^{2+} remaining in the solution and the accumulative CuI precipitate increases with progression of the accumulation. The minimum mass fractionation between the two phases is c. 40 $\varepsilon^{65}Cu$ units.

5. Mass fractionation during biological processes

Transition metals such as Fe, Cu, Zn, Cr, Ni and Mo are all reactive in biological systems [35–37]. Thus variations of transition metal isotope compositions may be important in tracing the interaction between geosphere and biosphere, and to trace the pathways of these elements into and within biological systems. A prerequisite of these applications is an adequate appreciation of possible mass fractionation processes of these isotopes during steps of biological uptake. In this study, a series of well-controlled culture growth experiments have been undertaken to investigate particular stages of biologically induced mass fractionation of Cu and Fe isotopes during uptake in vivo. Therefore, instead of looking at whole cell fractionation of isotopes as adopted in a previous study [11], an analysis of fractionation in the uptake into particular proteins which form kinetic traps for elements has been made. In addition, natural protein samples from some animals have also been analysed.

5.1. The uptake of Cu into a cellular protein azurin

This has been studied using two approaches. One was to examine Cu uptake in vitro from a known source directly into the apoprotein of azurin. The holoprotein was prepared by expression of the corresponding gene in a genetically

modified strain of *Escherichia coli* and isolating and purifying the protein according to published procedures [38,39]. The apoprotein was obtained from the purified holoprotein by removing the Cu. Details of the procedures have been described elsewhere [39]. This apoprotein was then exposed to $Cu(NO_3)_2$ aqueous solution of known isotope composition, and uptake was recorded in the copper azurin [38]. The other approach was an in vivo biological experiment, where the intact Cu protein azurin was synthesised directly inside cells of a bacterium. This was achieved by using a well-documented procedure by growing cells of *Pseudomonas aeruginosa* in a culture solution [40] with known copper isotope composition. The Cu protein azurin was then extracted and purified [38]. The purified Cu proteins were then decomposed by a series of treatments with concentrated $HClO_4$, and the Cu was isolated by ion exchange chromatography as described in Appendix A. All samples and source material $Cu(NO_3)_2$ were then transformed into chloride form before their analysis for Cu isotopes. Measured $^{65}Cu/^{63}Cu$ ratios are expressed in terms of $\varepsilon^{65}Cu$ units relative to reference material NIST 978.

Relative to the source material, the Cu isotope composition of the azurin expressed in *E. coli* is lighter by 15.3 $\varepsilon^{65}Cu$ units (Table 3). It should be emphasised that the copper uptake in vitro into the apoprotein of azurin is a kinetically controlled one-step process. The significant fractionation in Cu isotope compositions between this azurin and the source material shows that during biological processes not only the cell membranes can cause transition metal isotope fractionation as deduced from whole cell experiments [11], but that uptake into proteins within a single cell could also cause fractionation.

Relative to the source material, the Cu isotope composition of the azurin expressed directly in *P. aeruginosa* is lighter by 9.8 $\varepsilon^{65}Cu$ units (Table 3), 5.5 ε units smaller than that induced by copper uptake in vitro into the apoprotein of azurin. It should be pointed out that in this in vivo biological experiment, the copper uptake into the azurin consists of at least two steps: the uptake of copper from culture solution by the cell machinery, and the insertion of copper into the azurin. The

Table 3
Measurements of transition metal isotopes in biological samples

Sample	$\varepsilon^{56}Fe^a$	$\varepsilon^{57}Fe^a$	$\varepsilon^{65}Cu^b$	$\varepsilon^{66}Zn^c$	$\varepsilon^{67}Zn^c$	$\varepsilon^{68}Zn^c$
Ferredoxin-I expressed in *Azotobacter vinelandii*	−6.8	−9.9				
Culture solution after incubation	2.2	3.3				
FeCl$_3$, source material	2.1	3.0				
Azurin expressed in *E. coli*			−16.4			
Azurin expressed in *P. aeruginosa*			−10.9			
Cu(NO$_3$)$_2$, source material			−1.1			
Yeast Cu-metallothionein			−21.3			
Yeast Cu–Zn-superoxide dismutase			−16.0	10.8	16.3	21.0
CuSO$_4$, source material			−4.2			
Bovine haemoglobin	−26.8	−39.4				
Horse haemoglobin	−30.7	−44.9				
Pig haemoglobin	−33.5	−49.5				
Octopus haemocyanin			6.2			

[a] Measured $^{57}Fe/^{54}Fe$ and $^{56}Fe/^{54}Fe$ ratios are expressed as $\varepsilon^{57}Fe$ and $\varepsilon^{56}Fe$, which are deviations in parts per 10^4 from the Fe isotope reference material IRMM-14. See footnote of Table 1 for data precision.
[b] Measured $^{65}Cu/^{63}Cu$ ratio is expressed as $\varepsilon^{65}Cu$, which is deviation in parts per 10^4 from the Cu isotope reference material NIST-976. See footnote of Table 2 for data precision.
[c] Measured $^{66}Zn/^{64}Zn$, $^{67}Zn/^{64}Zn$ and $^{68}Zn/^{64}Zn$ ratios are expressed as $\varepsilon^{66}Zn$, $\varepsilon^{67}Zn$ and $\varepsilon^{68}Zn$, which are deviations in parts per 10^4 from an Aldrich standard solution. Repeated measurements of Romil Zn solution versus Aldrich Zn solution over a period of a few months give external precision of 0.5, 0.5 and 0.6ε at 2σ level for $\varepsilon^{66}Zn$, $\varepsilon^{67}Zn$ and $\varepsilon^{68}Zn$, respectively.

smaller mass fractionation observed in the in vivo experiment relative to the in vitro experiment may be interpreted as resulting from the preferential incorporation of lighter Cu isotope from this protein into subsequent proteins in the cell during the in vivo experiment. The two Cu uptake experiments together suggest that the transition metal isotopes fractionate along the uptake pathways within biological systems, i.e., stepwise fractionation.

5.2. The uptake of Cu proteins in yeast

Yeast cells were cultured in a solution [41] of known Cu isotope composition. Two proteins, Cu-metallothionein and Cu–Zn-superoxide dismutase (SOD), were extracted and purified from the cells [41]. Following decomposition and chemical purification, the protein samples and their source material CuSO$_4$ were measured for Cu isotopes [4]. SOD also contains zinc, and its zinc isotope composition has also been analysed using a standard sample bracketing approach similar to Cu isotope measurement. The measured $^{66}Zn/^{64}Zn$, $^{67}Zn/^{64}Zn$ and $^{68}Zn/^{64}Zn$ ratios are expressed in terms of $\varepsilon^{66}Zn$, $\varepsilon^{67}Zn$ and $\varepsilon^{68}Zn$, re-

spectively, which are deviations in parts per 10^4 from a Romil Zn standard solution (Table 3).

The Cu isotope fractionation induced by these two biological processes are similar in magnitude to those produced during Cu uptake into azurin (Table 3), and the proteins are isotopically lighter relative to their source. However, the Cu isotope composition in the Cu-metallothionein is lighter than the Cu–Zn-SOD by c. 5 $\varepsilon^{65}Cu$ units (Table 3). This difference in Cu isotope composition between two proteins from the same organism demonstrates again that mass fractionation of Cu isotopes occurs stepwise along the biological pathways within a single cell. This, together with the above two Cu uptake experiments, shows that the potential exists in using transition metal isotopes to trace the kinetic stepwise pathways of these elements within biological systems.

There is no known sequential uptake relationship between these two proteins. However, Cu in metallothionein is present as Cu^+ whereas Cu in the SOD is present as both Cu^+ and Cu^{2+}. As demonstrated in the last section, oxidation–reduction is an important controlling factor of Cu isotope fractionation. It is interesting that the difference in Cu isotope composition between the Cu-

metallothionein and the Cu–Zn-SOD is in the same sense as that seen during Cu reduction (Fig. 3A). It is worth pointing out that Cu was presented as Cu^{2+} in the culture solution. Thus the reduction of Cu^{2+} to Cu^+ must have taken place within the yeast cell.

5.3. The uptake of Fe into a protein ferredoxin

The uptake of Fe from a culture solution of known isotope composition into the proteins of *Azotobacter vinelandii*, from which one protein ferredoxin-I (*Av*FDI) was isolated and purified. The cells were grown in a 200 L fermentor for c. 18 h, and harvested in the mid log phase. Details of the experiment procedures have been published elsewhere [42,43]. Following decomposition and chemical purification as described above, Fe in the *Av*FDI, its Fe source $FeCl_3$, and the culture solution after *A. vinelandii* growth and removal have all been analysed for isotope composition, and the results are presented in Table 3. As for the Cu uptake biological experiments, Fe isotope composition in the *Av*FDI is lighter relative to its source. The mass fractionation measured between the protein and Fe source is 13.2 ε^{57}Fe units.

5.4. Fe and Cu isotope compositions in natural biological samples

In addition to the above in vivo and in vitro biological experiments studying unicellular organisms, some natural biological samples from multiple-cellular organism were also analysed for Cu and Fe isotopes. They are oxygen transporting proteins from higher organisms, including bovine, horse and pig haemoglobins and octopus hemocyanin. The hemocyanin was extracted from the blood of a Mediterranean Sea octopus, whereas the haemoglobin samples were purchased from Sigma®. As shown in Table 3, the Fe isotope compositions of haemoglobin samples fall into the range from −39.4 to −49.5 in ε^{57}Fe values relative to the isotope standard material IRMM-14. These are about four to five times lower than the ε^{57}Fe value measured in the *Av*FDI, and are the lowest ε^{57}Fe values obtained so far for a wide variety of terrestrial and extraterrestrial materials

[5,6,44]. Although the isotope compositions of the direct Fe sources of these high organisms are unknown, the Fe isotopes of their ultimate source are not expected to differ greatly from those of the standard reference material IRMM-14. This is because the Fe isotope compositions of loess ($-1 < \varepsilon^{57}$Fe < 5) [5] taken as representative of the continental crust, and the bulk meteorite samples ($-1 < \varepsilon^{57}$Fe < 3) [5,6] taken as representative of solar system are all very close to that of the standard used here. The Fe isotope difference between the haemoglobin samples from animals and the ferredoxin-I from the *A. vinelandii* is consistent with the expectation of isotope evolution along food chains.

Cu in octopus hemocyanin is derived from seawater. Thus its isotope composition may be regarded as a proxy of that of seawater. The Cu isotope composition obtained from this protein is heavier than that of the isotope standard material NIST-976 (Table 3). As it has been demonstrated for Cu and Fe isotopes above that organisms incorporate lighter isotopes of transition metals preferentially, the obtained result suggests that the Cu isotope composition in the Mediterranean seawater is likely to be heavier still.

6. Discussion and conclusions

This contribution amounts to a broadly-based study of mass fractionation in transition metal isotopes. It shows that Cu and Fe isotopes can be fractionated by a variety of geochemical, cosmochemical, chemical and biological processes. The results presented in this paper are expected to be of general significance for other transition metal isotopes, such as those of Zn, Ni, Cr, and Mo, as they have similar masses and show many similar chemical, geochemical and biochemical properties.

It is demonstrated that mass fractionation of transition metal isotopes occurs during a variety of equilibrium processes in different environments. These include simple ion exchange equilibrium processes between mineral phases at high temperatures and those between aqueous species at low temperatures, redox-related equilibrium

processes between mineral phases at high temperatures and those between inorganic species at low temperatures. This study therefore provides a decisive challenge as to the view that transition metal isotopes are too heavy to be fractionated significantly by equilibrium processes [3,11], and expands the scope of application of these new isotope systems greatly.

Oxidation–reduction processes are of fundamental importance in geochemistry, cosmochemistry and biochemistry. The experimental results on Cu isotopes presented in this study demonstrate unequivocally that large mass fractionation of transition metal isotopes can be produced by such a redox process, at least in low temperature environments. While the significance of these results should not be over-generalised, it is worthy pointing out that the observed mass fractionation of Fe isotopes between olivine and metal phases in pallasites is also redox-related in nature. The latter results show that such redox-related processes do induce mass fractionation of transition metal isotopes to a detectable level even at temperatures high enough to produce melts. Furthermore, the difference in Cu isotope composition between Cu-metallothionein and the Cu–Zn-SOD of the same organism indicates that oxidation–reduction taking place within biological systems is likely to play a considerable role in transition metal isotope fractionation during biological processes. All together, these imply that variations of isotope abundances of transition metals with multiple valence states have the potential to throw light on some important redox-related processes taking place in natural systems.

Geosphere–biosphere interaction is a subject of great interest in both the Earth and biological sciences. The roles played by organisms in mineralisation, weathering and climate change, and the effects inserted by the availability of nutrition elements on biological productivity have been increasingly recognised [45–48]. A possibility for the understanding of the interaction between geosphere and biosphere lies in the use of natural tracers to detect the processes and pathways involved. Transition metals such as Fe, Cu, Zn, Cr, Ni, and Mo are all biologically utilised [35–37]. These elements provide important linkages in nat-

ural processes between inorganic and biological chemistry. Results obtained in this study show that mass fractionation of transition metal isotopes can be induced to a considerable level by biological processes, and that biological activities take up light isotopes preferentially. Thus transition metal isotopes offer the potential to trace key pathways of geosphere–biosphere interaction.

Understanding the pathways of transition metals within biological systems is of great importance in biological and medical sciences, as they are biological nutrients. The experiments in this study demonstrate that mass fractionation of transition metal isotopes occurs stepwise along the biological pathways. This suggests that it is feasible to use these new isotope systems to trace the kinetic stepwise pathways of nutrients such as Fe, Cu and Zn within biological systems.

Appendix A. Chemical separation and plasma source mass spectrometry

A1. Chemical separation

All samples used in this study were chemically purified by ion exchange chromatographic separation following complete digestion. Methods used for sample digestion vary according to the different nature of samples as described in the main text. AG MP-1 resin of 100–200 mesh is used for Cu, Fe and Zn separation, using an approach similar to that described previously [2]. Before loading, all samples were treated with H_2O_2 and dissolved in 6 M HCl.

For Cu separation, samples were loaded and eluted with 6 M HCl. Although this resin may induce large mass fractionation during the chromatography (Fig. 2 and [2]), replicates of both

natural samples and standard solutions show that the purification process causes no detectable Cu isotope fraction as 100% recovery is achieved, which is consistent with a previous study [2].

For Fe separation, samples were loaded and first washed with 6 M HCl to remove ions other than Fe and Zn, then 2 M HCl was used to strip Fe. Isotope fractionation of up to $\sim 40\varepsilon$ in $^{57}Fe/^{54}Fe$ ratio between the fractional collections during Fe elution has been observed, similar to a previous study [16]. However, 100% Fe yield is achieved, and replicates of samples and standard solution show no detectable fractionation induced by the purification process (Table 4).

A2. Fe isotope mass spectrometry

The techniques reported here focus on high precision measurement of $^{56}Fe/^{54}Fe$ and $^{57}Fe/^{54}Fe$ ratios only, as ^{58}Fe is very small (0.33 at%) and the cones of the plasma source mass spectrometer are made of Ni, which has ^{58}Ni.

A2.1. Sample introduction and interfering signal suppression

For Fe isotope measurement using plasma source mass spectrometry, the potential problem of matrix effects, and monatomic interferences, such as ^{54}Cr on ^{54}Fe, are reduced to a negligible level by chemical purification. However, the molecular spectral inferences such as $[ArN]^+$ and $[ArO]^+$ need to be dealt with through techniques of mass spectrometry. This has been done by a combination of three approaches:

Firstly, samples and standards are introduced into the mass spectrometer in dilute (0.1 M) HCl solutions through a modified CeTac MCN6000 desolvating nebuliser, which is operated without N_2 flow as described before [7]. This approach significantly reduces the supply of both O and N to the Ar plasma.

Secondly, the spectral interference signals are further suppressed by introducing sample and standard solutions at increased Fe concentrations. Of primary concern for the interfering signals are their intensities relative to those of Fe isotopes. Thus the spectrally interfering signals may be suppressed relatively by increasing the Fe concentrations of both samples and standards. This is achieved by collecting $^{56}Fe^+$ signal in a Faraday equipped with a 10^{10} Ω resistor rather than the 10^{11} Ω used for the rest. In this study, solutions of c. 20 ppm Fe were used.

Thirdly, the effects of the molecular interferences on Fe isotopes are further minimised by matching concentrations of Fe in standard and sample solutions closely. The standard–sample bracketing procedure has been used during this study. By expressing the Fe isotope composition of samples relative to that of a standard, much of the bias in measurements resulting from molecular interferences cancel out, provided that the Fe concentrations of standard and sample are matched closely enough. The accuracy to which the Fe concentrations must be matched depends upon the intensities of spectrally interfering signals relative to those of Fe isotopes, and upon the precision the instrument may achieve. In this study, concentrations of Fe in standard and sample solutions were matched to within 20%.

Table 4
Replicates of Fe purification of meteorite samples and a standard solution

Experiment no.	Description	$\varepsilon^{56}Fe^a$	$\varepsilon^{57}Fe^a$	Sample no.	Description	$\varepsilon^{56}Fe^b$	$\varepsilon^{57}Fe^b$
YG-A1	Aldrich Fe	0.1	0.2	Mt180-2	Forest City (H5)[c]	−0.6	−0.8
YG-A2	Aldrich Fe	−0.1	0	Mt180-2a	duplicate[c]	−0.4	−0.6
YG-A3	Aldrich Fe	−0.1	−0.1	Mt1-1	Pallasite Krasnojarsk[c]	−0.9	−1.3
YG-A4	Aldrich Fe	0.2	0.3	Mt1-1a	Duplicate[c]	−1.1	−1.5

[a] Relative to the original Aldrich Fe solution.
[b] Relative to IRMM-14 Fe isotope reference material.
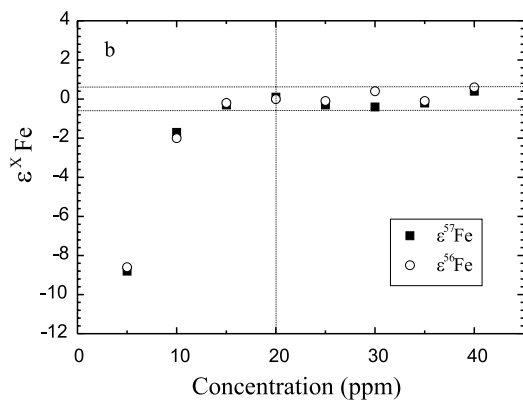[c] Data have been published previously [6].

Fig. 4. Measurement of ε^{56}Fe and ε^{57}Fe values in Romil 'sample' Fe solutions with concentration ranging from 5 to 40 ppm, relative to Romil 'standard' Fe solution at 20 ppm. The two dotted horizontal lines bracket the measurement repeatability at 2σ level as defined in Fig. 6. The dotted vertical line indicates the Fe concentration in the 'standard' Romil solution.

A2.2. Interference assessment

Although the molecular interfering signals are suppressed greatly using the approaches described above, the extents of the effect of these interfering molecules on the measured Fe isotope compositions of samples have been thoroughly investigated.

Firstly, the intensities of molecular interfering signals on Fe isotopes have been determined using an Fe-free 0.1 M HCl solution, and are typically c. 10^{-14}, 2×10^{-14} and $<10^{-17}$ A at 54, 56 and 57 amu, respectively. Under optimised conditions observed signal intensities for ^{54}Fe$^+$, ^{56}Fe$^+$ and ^{57}Fe$^+$ of a 20 ppm Fe solution are typically c. 5×10^{-11}, 9×10^{-10} and 2×10^{-11} A, respectively. Thus the contributions of interfering molecular signals are c. 200, 20 and <1 ppm at the measured ^{54}Fe$^+$, ^{56}Fe$^+$ and ^{57}Fe$^+$ signals, respectively. The intensities of these interfering signals are constant during the same run, but may vary slightly with different instrumental set ups.

Secondly, the effects of the interfering molecular signals on the measured Fe isotope compositions of samples have been examined by measuring solutions of different Fe concentrations. Fig. 4 shows the results of a series of measurements of ε^{56}Fe and ε^{57}Fe in Romil 'sample' solutions with

different Fe concentrations, relative to Romil 'standard' Fe solution at 20 ppm. The Romil 'sample' Fe solutions used vary from 5–40 ppm. These results demonstrate that: (1) the true ε^{56}Fe and ε^{57}Fe values can be obtained when the Fe concentrations in both sample and standard solution are identical; (2) the extent to which the Fe concentration of a sample may be varied relative to that of the standard depends upon the relative intensity of the interfering signal and the analytical precision. Also, from Fig. 4 it can be deduced that the concentrations of Fe in sample and standard solutions may differ by $\pm 30\%$ with a negligible introduction of error into the ε^{57}Fe value relative to the measurement repeatability achieved (see A2.4).

A2.3. Valence effects

The possibility that the oxidation state of Fe in a sample or standard solution may affect the instrumental mass fractionation should be addressed, since observation shows that the measurements of the isotope composition of the same Fe solution in dilute HCl vary significantly after standing for a period of months. This issue has been investigated by measuring the Fe isotope ratios of a series of solutions in 0.1 M HCl where Fe^{2+} and Fe^{3+} coexist relative to those of the corresponding Fe solutions where only Fe^{3+} presents, and the results are expressed as $\Delta\varepsilon^{X}$Fe. Presence of Fe^{2+} in the mixed valence solutions is verified by the characteristic red coloration that followed the addition of 2,2′-bipyridine solution. The measured isotope differences between the mixed valence solutions and their corresponding Fe^{3+} solutions, together with the coloration of the mixed valence solutions, are shown in Fig. 5. These results demonstrate that the valence state of Fe in the final solutions has a significant effect on instrumental isotope fractionation.

The problem of valence effects on instrumental mass fractionation of Fe isotopes can be eliminated by ensuring that all Fe in both sample and standard solutions be in the same valence state. This can be achieved by oxidising both the standard and samples to Fe^{3+} using H_2O_2, and subsequent elimination of the excess H_2O_2 by dry-
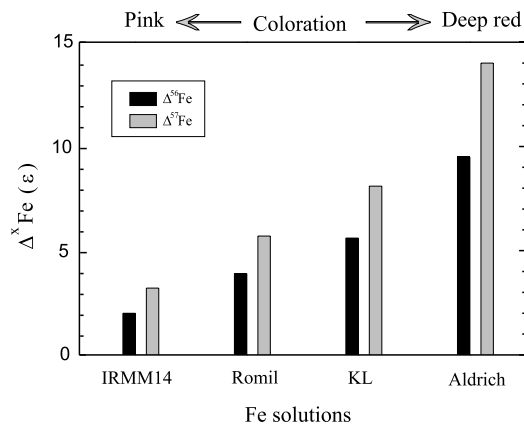
Fig. 5. A plot showing the measured Fe isotope compositions of mixed valence solutions relative to their corresponding solutions where only Fe^{3+} exists. The coloration of the mixed valence solution when 2,2′-bipyridine is added are also plotted. A deeper red colour implies more Fe^{2+} in a solution.

ing the solutions down. Standards and samples are redissolved in 0.1 M HCl prior to introduction into the mass spectrometry. Observations also show that in the 0.1 M HCl medium the reduction of Fe^{3+} to Fe^{2+} causes no detectable effect on instrumental mass fractionation over a period of a week.

A2.4. Data acquisition

Signals of the four Fe isotopes are simultaneously collected. The correction of instrumental mass discrimination is made relative to a standard reference material using the standard-sample bracketing technique. The results are expressed as:

$$\varepsilon^X Fe = [(^X Fe/^{54}Fe)_{sample}/(^X Fe/^{54}Fe)_{standard} - 1] \times$$

$$10000$$

where X denotes 56 or 57.

Samples and standards were measured alternatively. Runs of sample and standard were separated by washes using 2 M HCl for 5 min and 0.1 M HCl for 2 min. Data were acquired in blocks of 10 ratios with 10-s integration times, and background measurements were taken for 20 s prior to each data block.

To ascertain any contribution from Cr^+ to the measured $^{54}Fe^+$ signal, Cr is routinely monitored at $^{52}Cr^+$ for both samples and standards. In no case has the contribution been found to be significant.

A2.5. Repeatability and precision

The performance of the instrument for Fe isotope analysis has been assessed by repeated measurement of Romil Fe standard solutions against Fe isotope reference material IRMM-14 using the techniques described above. Results obtained over a period of 20 months are presented in Fig. 6. The average Fe isotope values obtained for Romil Fe are $\varepsilon^{56}Fe = 1.8 \pm 0.4$ (2 S.D.) and $\varepsilon^{57}Fe = 2.8 \pm 0.6$ (2 S.D.). These results are indistinguishable from the $\varepsilon^{57}Fe$ value of 2.5 ± 0.8 (2 S.D.) for Romil Fe obtained previously [7], where only the $^{57}Fe/^{54}Fe$ ratio was measured. The long-term repeatability obtained in this study defines an external precision of 0.4 and 0.6 ε units for $^{56}Fe/^{54}Fe$ and $^{57}Fe/^{54}Fe$ measurements, respectively, at 95% confidence (2σ) level. As documented above, variations in $\varepsilon^{56}Fe$ and $\varepsilon^{57}Fe$ of natural samples after replicated column processing are all within the precision reported here (Table 4).
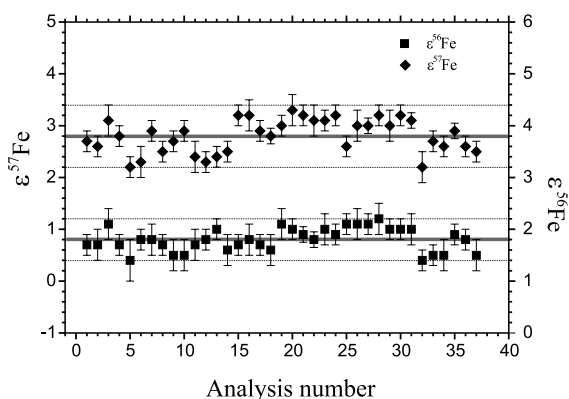

Fig. 6. Repeatability of $^{56}Fe/^{54}Fe$ and $^{57}Fe/^{54}Fe$ measurements. Romil Fe solution relative to IRMM-14 Fe isotope reference standard. The average Fe isotope values obtained for Romil over a period of 20 months are $\varepsilon^{56}Fe = 1.8 \pm 0.4$ (2 S.D.) and $\varepsilon^{57}Fe = 2.8 \pm 0.6$ (2 S.D.). This long-term repeatability is used to define an external precision of 0.4 ε units for $^{56}Fe/^{54}Fe$ and 0.6 ε units for $^{57}Fe/^{54}Fe$ measurements at 2σ level.

References

[1] A.N. Halliday, D.C. Lee, J.N. Christensen, M. Rehkamper, W. Li, X. Luo, C.M. Hall, C.J. Ballentine, T. Pettlee, C. Stirling, Applications of multiple collector ICPMS to cosmochemistry, geochemistry and paleoceanography, Geochim. Cosmochim. Acta 62 (1998) 919–940.

[2] C.N. Maréchal, P. Télouk, F. Albarède, Precise analysis of copper and zinc isotopic compositions by plasma-source mass spectrometry, Chem. Geol. 156 (1999) 251–273.

[3] B.L. Beard, C.M. Johnson, High precision iron isotope measurements of terrestrial and lunar materials, Geochim. Cosmochim. Acta 63 (1999) 1653–1660.

[4] X.K. Zhu, R.K. O'Nions, Y. Guo, N.S. Belshaw, D. Rickard, Determination of natural Cu-isotope variation by plasma-source mass spectrometry: implications for use as geochemical tracers, Chem. Geol. 163 (2000) 139–149.

[5] X.K. Zhu, R.K. O'Nions, Y. Guo, B.C. Reynolds, Secular variation of iron isotopes in North Atlantic deep water, Science 287 (2000) 2000–2002.

[6] X.K. Zhu, R.K. O'Nions, Y. Guo, E.D. Young, R.D. Ash, Isotope homogeneity of iron in the early solar nebula, Nature 412 (2001) 311–313.

[7] N.S. Belshaw, X.K. Zhu, Y. Guo, R.K. O'Nions, High precision measurement of iron isotopes by plasma source mass spectrometry, Int. J. Mass Spectrom. Ion Phys. 197 (2000) 191–195.

[8] A.D. Anbar, K.A. Knab, J. Barling, Precise determination of mass-dependent variations in the isotopic composition of molybdenum using MC-ICPMS, Anal. Chem. 73 (2001) 1425–1431.

[9] C. Siebert, T.F. Nägler, J.D. Kramers, Determination of molybdenum isotope fractionation by double-spike multi-collector inductively coupled plasma mass spectrometry, Geochem. Geophys. Geosyst. 2 (2001) 2000GC000124.

[10] J. Barling, G.L. Arnold, A.D. Anbar, Natural mass-dependent variations in the isotopic composition of molybdenum, Earth Planet. Sci. Lett. 193 (2001) 447–457.

[11] B.L. Beard, C.M. Johnson, L. Cox, K.H. Nealson, C. Aguilar, Iron isotope biosignatures, Science 285 (1999) 1889–1892.

[12] C.N. Maréchal, E. Nicolas, C. Douchet, F. Albarède, Abundance of zinc isotopes as a marine biogeochemical tracer, Geochem. Geophys. Geosyst. 1 (2000) 1999GC000029.

[13] T.D. Bullen, A.F. White, C.W. Childs, D.V. Vivit, M.S. Schulz, Demonstration of significant abiotic ion isotope fractionation, Geology 29 (2001) 699–702.

[14] K.W. Mandernack, D.A. Bazylinski, W.C. Hanks, T.D. Bullen, Oxygen and iron isotope studies of magnetite produced by magnetic bacteria, Science 285 (1999) 1892–1895.

[15] S.L. Brantley, L. Liermann, T.D. Bullen, Fractionation of Fe isotopes by soil microbes and organic acids, Geology 29 (2001) 535–538.

[16] A.D. Anbar, J.E. Roe, J. Barling, K.H. Nealson, Non-biological fractionation of iron isotopes, Science 288 (2000) 126–128.

[17] A. Matthews, X.K. Zhu, K. O'Nions, Kinetic iron stable isotope fractionation between iron (-II) and (-III) complexes in solution, Earth Planet. Sci. Lett. 192 (2001) 81–92.

[18] E.A. Schauble, G.R. Rosman, H.P. Taylor Jr., Theoretical estimates of equilibrium Fe-isotope fractionations from vibrational spectroscopy, Geochim. Cosmochim. Acta 65 (2001) 2487–2497.

[19] V.B. Polyakov, S.D. Mineev, The use of Mössbauer spectroscopy in stable isotope geochemistry, Geochim. Cosmochim. Acta 64 (2000) 849–865.

[20] A.L. Littlejohn, H.J. Greenwood, Lherzolite nodules in basalts from British Columbia, Canada, Can. J. Earth Sci. 11 (1974) 1288–1308.

[21] T. Fujii, C.M. Scarfe, Petrology of ultramafic nodules from Boss Mountain, central British Columbia, Geol. Assoc. Can./Min. Assoc. Can. Abstr. Prog. 6 (1981) A20.

[22] D. Canil, D. Virgo, C.M. Scarfe, Oxidation state of mantle xenoliths from British Columbia, Canada, Contrib. Mineral. Petrol. 104 (1990) 453–462.

[23] J.B. Dawson, J.V. Smith, Metasomatised and veined upper-mantle xenoliths from Pello Hill, Tanzania: evidence for anomalously-light mantle beneath the Tanzanian sector of the East African Rift Valley, Contrib. Mineral. Petrol. 100 (1988) 510–527.

[24] D. Mattey, D. Lowry, C. Macpherson, Oxygen isotope composition of mantle peridotite, Earth Planet. Sci. Lett. 128 (1994) 231–241.

[25] H.C. Urey, The thermodynamic properties of isotopic substances, J. Chem. Soc. (1947) 562–581.

[26] R.E. Criss, Principles of Stable Isotope Distribution, Oxford University Press, New York, 1999, 254 pp.

[27] K. Robards, P.R. Haddad, P.E. Jacson, Principles and Practice of Modern Chromatographic Methods, Academic Press, London, 1994, 495 pp.

[28] E. Glueckauf, Theory of chromatography. Part 9. The 'theoretical plate' concept in column separation, Trans. Faraday Soc. 51 (1955) 34–44.

[29] E. Glueckauf, Theory of chromatography. Part 11. Enrichment of isotopes by chromatography, Trans. Faraday Soc. 54 (1958) 1203–1205.

[30] A.W. Russell, D.A. Papanatassiou, Calcium isotope fractionation in ion-exchange chromatography, Anal. Chem. 50 (1978) 1151–1154.

[31] J. Bjerrum, L.H. Skibsted, Weak chloro complex-formation by Cu(II) in aqueous chloride solutions, Inorg. Chem. 25 (1986) 2479–2481.

[32] R.W. Ramette, Copper(II) complexes with chloride-ion, Inorg. Chem. 25 (1986) 2481–2482.

[33] T.N. Van der Walt, F.W.E. Strelow, R. Verheij, The influence of crosslinkage on the distribution coefficients and anion-exchange behaviour of some elements in hydrochloric-acid, Solvent Extr. Ion Exch. 3 (1985) 723–740.

[34] R.C. Weast, CRC Handbook of Chemistry and Physics, CRC Press, Cleveland, OH, 1976, F-352 pp.

[35] J.J.R. Frausto da Silva, R.J.P. Williams, The Biological Chemistry of the Elements, Oxford University Press, Oxford, 1997, 561 pp.

[36] R.J.P. Williams, J.J.R. Frausto da Silva, The Natural Selection of the Chemical Elements, Oxford University Press, Oxford, 1996, 646 pp.

[37] R.J.P. Williams, J.J.R. FraustodaSilva, The distribution of elements in cells, Coordin. Chem. Rev. 200–202 (2000) 247–348.

[38] M. VandeKamp, F.C. Hali, A.F. Rosato, G.W. Canters, Purification and characterisation of a nonreconstitutable azurin obtained by heterologous expression of the *Pseudomonas aeruginosa azu* gene in *Escherichia coli*, Biochim. Biophys. Acta 1019 (1990) 283–292.

[39] H. Nar, A. Messerschmidt, R. Huber, M. vandeKamp, G.W. Canters, Crystal structure of Pseudomonas areuginosa apo-azurin at 1.85 Å resolution, FEBS Lett. 306 (1992) 119–124.

[40] J. Sambrook, E.F. Fritsch, T. Maniatis, Molecular Cloning: A Laboratory Manual, Cold Spring Harbor Laboratory Press, Cold Spring JHarbor, NY, 1989, pp. 18–88.

[41] U. Weser, H.J. Hartmann, Purification of yeast copper-metallothionein, Methods Enzymol. 205 (1991) 274–278.

[42] P.J. Stephens, G.M. Jensen, F.J. Devlin, T.V. Morgan, C.D. Stout, A.E. Martin, B.K. Burgess, Circular-dichroism and magnetic circular-dichroism of *Azotobacter vinelandii* ferredoxin-I, Biochemistry 30 (1991) 3200–3209.

[43] A. Vazquez, B. Shen, K. Negaard, S. Iismaa, B. Burgess, Overexpression of perredoxin-I in Azotobacter-vinelandii, Protein Expres. Purif. 5 (1994) 96–102.

[44] X.K. Zhu, N.S. Belshaw, Y. Guo, R.K. O'Nions, Natural variations of iron and copper isotopes determined by plasma source mass spectrometry: applications to geochemistry and cosmochemistry, Ninth Annual V.M. Goldschmidt Conference, LPI Contribution No. 971, Houston, TX, 1999, 341 pp.

[45] J. Akai, K. Akai, M. Ito, S. Nakano, Y. Maki, I. Sasagawa, Biologically induced iron ore at Gunma iron mine, Japan, Am. Mineral. 84 (1999) 171–182.

[46] B.E. Kalinowski, L.J. Liermann, S. Givens, S.L. Brantley, Rates of bacteria-promoted solubilisation of Fe from minerals: a review of problems and approaches, Chem. Geol. 169 (2000) 357–370.

[47] J.H. Martin, Glacial-interglacial CO_2 changes: the iron hypothesis, Paleoceanography 5 (1990) 1–13.

[48] M. Ledin, Accumulation of metals by microorganism – processes and importance for soil systems, Earth-Sci. Rev. 51 (2000) 1–31.